MOLECULAR PHARMACOLOGY

Sustained Formation of Nitroglycerin-Derived Nitric Oxide by Aldehyde Dehydrogenase-2 in Vascular Smooth Muscle Without Added Reductants

Implications for the Development of Nitrate Tolerance

Marissa Opelt, Gerald Wölkart, Emrah Eroglu, Markus Waldeck-Weiermair, Roland Malli, Wolfgang F. Graier, Alexander Kollau, John T. Fassett, Astrid Schrammel, Bernd Mayer, and Antonius C.F. Gorren

Supplementary Material

Contents

Kinetic analysis of the NO concentration time courses

Derivation of the fitting equations

In the absence of DTT the reaction of GTN with ALDH2 was originally assumed to yield only one equivalent of NO concomitant with the oxidation of the catalytically active cysteine residue C302 (Rxn 1),

$$GTN + ALDH2_{red} \dashrightarrow NO + ALDH2_{ox} \qquad \text{(Rxn 1)}$$

with suffices 'red' and 'ox' indicating the redox state of C302. This is a pseudo-first order reaction when [GTN] >> [ALDH2]. Decay of NO is expected to be a first-order process as well (Rxn 3),

$$NO \dashrightarrow X \qquad \text{(Rxn 3)}$$

where 'X' may be any unspecified reaction product in addition to disappearance of NO with the perfusion solution after diffusion out of the cell. Combined, these two reactions are a set of two consecutive irreversible first-order reactions, for which Eq. 1 gives the exact solution:

$$[\mathrm{NO}]_t = [\mathrm{ALDH2_{red}}]_0 \bullet \frac{k_{\mathrm{ox}}}{k_{\mathrm{dec}} - k_{\mathrm{ox}}} \bullet \left(e^{-k_{\mathrm{ox}} \bullet t} - e^{-k_{\mathrm{dec}} \bullet t}\right) \qquad \text{(Eq. 1)}$$

In this and subsequent equations k_{ox} represents the pseudo-first-order rate constants of Rxn 1 ($k_{ox} = k_{Rxn1} \bullet [GTN]$) and k_{dec} is the first-order rate constant of Rxn 3 ($k_{dec} = k_{Rxn3}$).

In the presence of DTT, $ALDH2_{red}$ will be regenerated from $ALDH2_{ox}$, resulting in catalytic zero-order formation of NO from GTN (Rxn 4), which will again be followed by first-order disappearance of NO (Rxn 3).

$$NO \xrightarrow{ALDH2} X \,(\textit{zero-order}) \qquad \text{(Rxn 4)}$$

$$NO \dashrightarrow X \qquad \text{(Rxn 3)}$$

This set of reactions is exactly described by Eq. 2,

$$[\mathrm{NO}]_t = \frac{v_{\mathrm{cat}}}{k_{\mathrm{dec}}} \bullet \left(1 - e^{-k_{\mathrm{dec}} \bullet t}\right) \qquad \text{(Eq. 2)}$$

with v_{cat} representing the zero-order rate of NO formation by Rxn 4.

The decay of the NO signal after termination of perfusion was assumed to be a first-order process (Rxn 3). However, as discussed in the Results of the main text, the NO signal did not completely return to zero. To account for this we added a constant term to the single-exponential decay yielding fitting Eq. 3,

$$[\mathrm{NO}]_t = \Delta[\mathrm{NO}] \bullet e^{-k_{\mathrm{dec}} \bullet t} + [\mathrm{NO}]_\infty \qquad \text{(Eq. 3)}$$

with Δ[NO] representing the amplitude of the NO decay and $[\mathrm{NO}]_\infty$ the final level of NO.

Eq. 1 did not give satisfactory results for the reaction in the absence of DTT, as it failed to account for the continuous low-level generation of NO that follows the initial burst phase (not shown). Therefore, we adopted a three-reaction model that allows for regeneration of $ALDH2_{red}$ by an unspecified cellular reductant 'R' (Rxns 1-3):

$$GTN + ALDH2_{red} \dashrightarrow NO + ALDH2_{ox} \qquad \text{(Rxn 1)}$$

$$R_{red} + ALDH2_{ox} \dashrightarrow R_{ox} + ALDH2_{red} \qquad \text{(Rxn 2)}$$

$$NO \dashrightarrow X \qquad \text{(Rxn 3)}$$

As we did not have an exact solution to this set of equations, we combined the rate equation for the expected burst phase (Rxns. 1&3, Eq. 1) and the rate equation for the steady-state phase (Rxns. 4&3, Eq. 2), with a corrected expression for v_{cat} to account for the gradual conversion from the burst phase into the steady-state phase (Eq. 4):

$$[\mathrm{NO}]_t = \frac{v_{\mathrm{cat}}'}{k_{\mathrm{dec}}} + \frac{k_{\mathrm{ox}}[\mathrm{ALDH2_{red}}]_0}{k_{\mathrm{dec}} - k_{\mathrm{ox}}} e^{-k_{\mathrm{ox}} \bullet t} - \left(\frac{v_{\mathrm{cat}}'}{k_{\mathrm{dec}}} + \frac{k_{\mathrm{ox}}[\mathrm{ALDH2_{red}}]_0}{k_{\mathrm{dec}} - k_{\mathrm{ox}}} \right) e^{-k_{\mathrm{dec}} \bullet t}$$

$$\text{with} \quad v_{\mathrm{cat}}' = v_{\mathrm{cat}}(1 - e^{-k_{\mathrm{ox}} \bullet t}) \qquad \text{(Eq. 4)}$$

Since this same set of reactions is expected to describe the process in the presence of DTT, with DTT as R_{red}, we applied Eq. 4 to those time courses as well.

Validation of the fitting equations

To check the validity of Eq. 4, we performed a series of simulations of Rxns 1-3 (with the Tenua program (http://bililite.com/tenua) and fitted the results to Eq. 4 (Fig. S1). We obtained excellent agreement between the simulated and fitted parameters when steady-state NO generation was slow compared to the burst phase, but fitting parameters became less accurate when the rate of the reductive half-reaction approached or surpassed the rate of the oxidative half-reaction, even though the fitted curves still mimicked the simulated ones very well (Table S1). This is probably due to the fact that the burst phase gradually disappears when the rate of re-reduction of $ALDH2_{ox}$ increases and the oxidative half-reaction becomes rate determining. Consequently, Eq. 2 becomes the better choice under those conditions. Indeed, a fit of the simulated data with $k_{red} = 1 \cdot 10^6$ $M^{-1}s^{-1}$ (the purple line in Fig. S1) to Eq. 2 yielded parameters k_{dec} = 0.0207 s^{-1} (simulated value: 0.02 s^{-1}) and v_{cat} = 1.004 nM/s (simulated value 0.990 nM/s) with R = 0.99994 (not shown).

The comparison between simulated and fitted parameters shows that Eq. 4 is suitable at low rates of $ALDH_{ox}$ reduction, i.e. in the absence of DTT. At higher reduction rates the simpler Eq. 2 is preferable. However, the results also demonstrate that there is an intermediate range, represented by the orange curve in Fig. S1 where neither equation performs particularly well although very good fits were obtained with both equations. The reason appears to be that the rather featureless curves in this range are overdetermined by the full set of parameters, even though all four do contribute significantly to the reaction.

As a further test we simulated a number of curves with values for the rate constants in the range observed for the time course in the absence of DTT in Fig. 4 of the main text. In this range Eq. 4 was shown to perform very well (Fig. S2 and Table S2).

In Fig. S3 simulated time courses of NO formation and $ALDH_{red}$ oxidation are compared. This figure illustrates that the slow establishment of a constant NO concentration should not be confused with the faster formation of steady-state enzyme catalysis.

Figure S1. Simulation of time traces for ALDH2-catalyzed NO generation from GTN.

NO time traces were simulated for a 3-step model consisting of the oxidation of active site Cys of ALDH2 by GTN, yielding NO (reaction 1 with rate constant k_{ox}), regeneration of the reduced active site Cys by an endogenous reductant R (reaction 2 with rate constant k_{red}), and decay of the NO concentration (reaction 3 with rate constant k_{dec}).

$$GTN + ALDH2_{red} \dashrightarrow NO + ALDH2_{ox} \qquad (Rxn\ 1;\ k_{ox})$$

$$R_{red} + ALDH2_{ox} \dashrightarrow R_{ox} + ALDH2_{red} \qquad (Rxn\ 2;\ k_{red})$$

$$NO \dashrightarrow X \qquad (Rxn\ 3;\ k_{dec})$$

Simulations were carried out for a range of values for k_{red} and fixed values of all other parameters: $[GTN]_0$: 10^{-6} M, except Sim 5: 10^{-5} M; $[R_{red}]_0$: 10^{-5} M except Sim 1: 0 M; $[ALDH2_{red}]_0$: 10^{-8} M; k_{ox}: 10^5 $M^{-1}s^{-1}$ except Sim 5: 10^4 $M^{-1}s^{-1}$; k_{dec}: 0.02 s^{-1}; k_{red}: Sim 1: irrelevant.; Sim 2: $2\bullet10^2$ $M^{-1}s^{-1}$; Sim 3: 10^3 $M^{-1}s^{-1}$; Sim 4: $2\bullet10^3$ $M^{-1}s^{-1}$; Sim 5: 10^6 $M^{-1}s^{-1}$. Reaction 2 was omitted for simulation 1 ($[R_{red}]\bullet k_{red} = 0$). For Simulation 5 the concentration of GTN was increased 10-fold to prevent depletion of GTN within 300 s; to keep the product of $[GTN]_0$ and k_{ox} (i.e. the rate of Rxn 1) constant, k_{ox} was lowered 10-fold concomitantly. The simulated curves were then fitted to Eq. 4. The fitted curves (which largely coincide with the simulated curves) are shown as black dashed lines. Fitting parameters obtained by this procedure are compared with the simulation parameters in Table S1.

Figure S2. Simulated time traces for ALDH2-catalyzed NO generation from GTN with parameters derived from the observed time traces.

Simulations were performed as for Fig. S1 with parameters: $[GTN]_0$: 10^{-6} M; $[R_{red}]_0$: 10^{-6} M; $[ALDH2_{red}]_0$: $3.3\bullet10^{-8}$ M; k_{ox}: $2.58\bullet10^4$ $M^{-1}s^{-1}$; k_{dec}: 0.0378 s^{-1}; k_{red}: as indicated in the figure. The simulated curves were then fitted to Eq. 4. The fitted curves (which largely coincide with the simulated curves) are shown as black dashed lines. Fitting parameters obtained by this procedure are compared with the simulation parameters in Table S2.

Figure S1

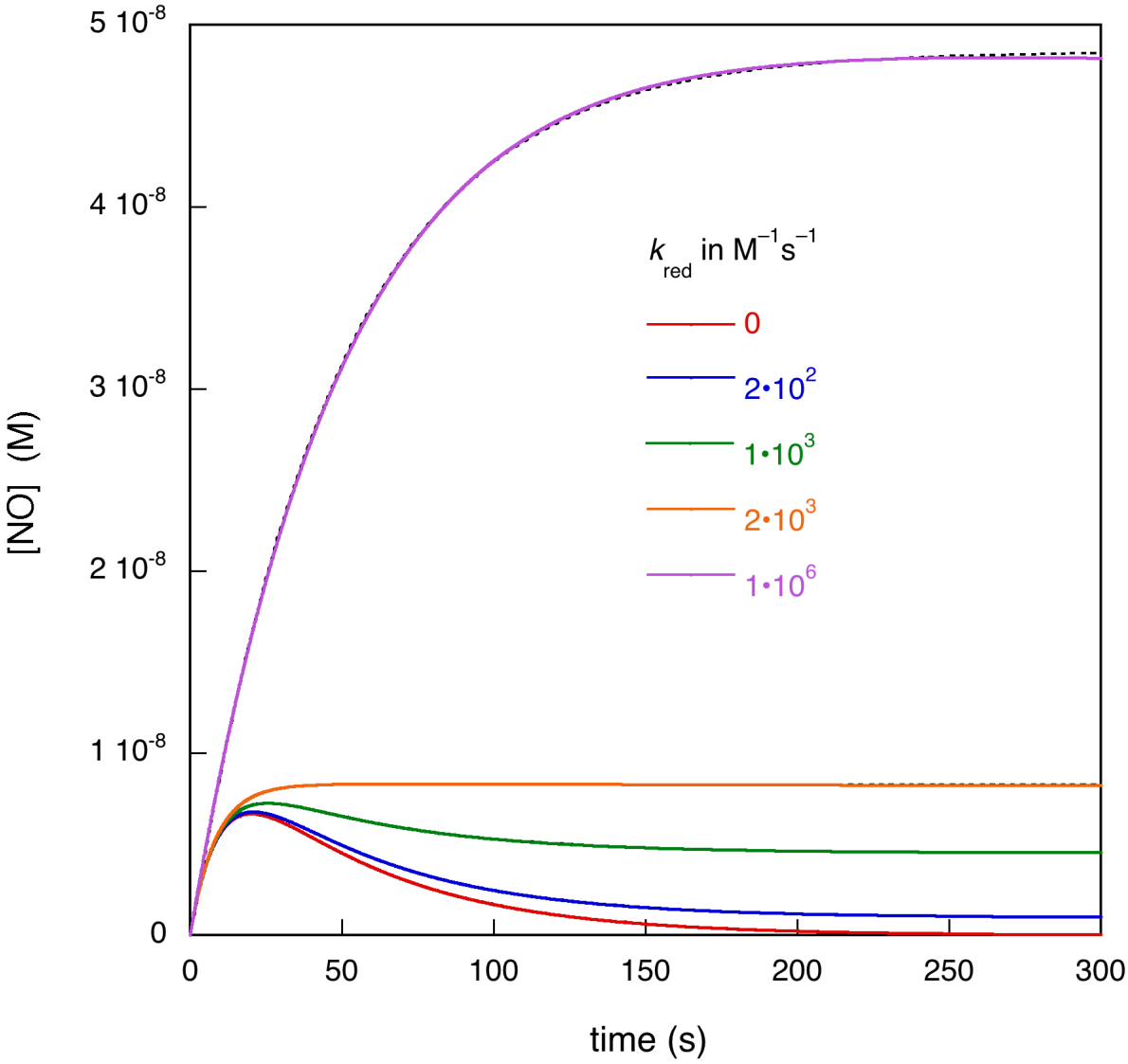
5 10-8
4 10-8
3 10-8
2 10-8
1 10-8
0
[NO] (M)
0
50
100
150
200
250
300
time (s)
k red in M−1s−1
0
2•10^2
1•10^3
2•10^3
1•10^6

Figure S2

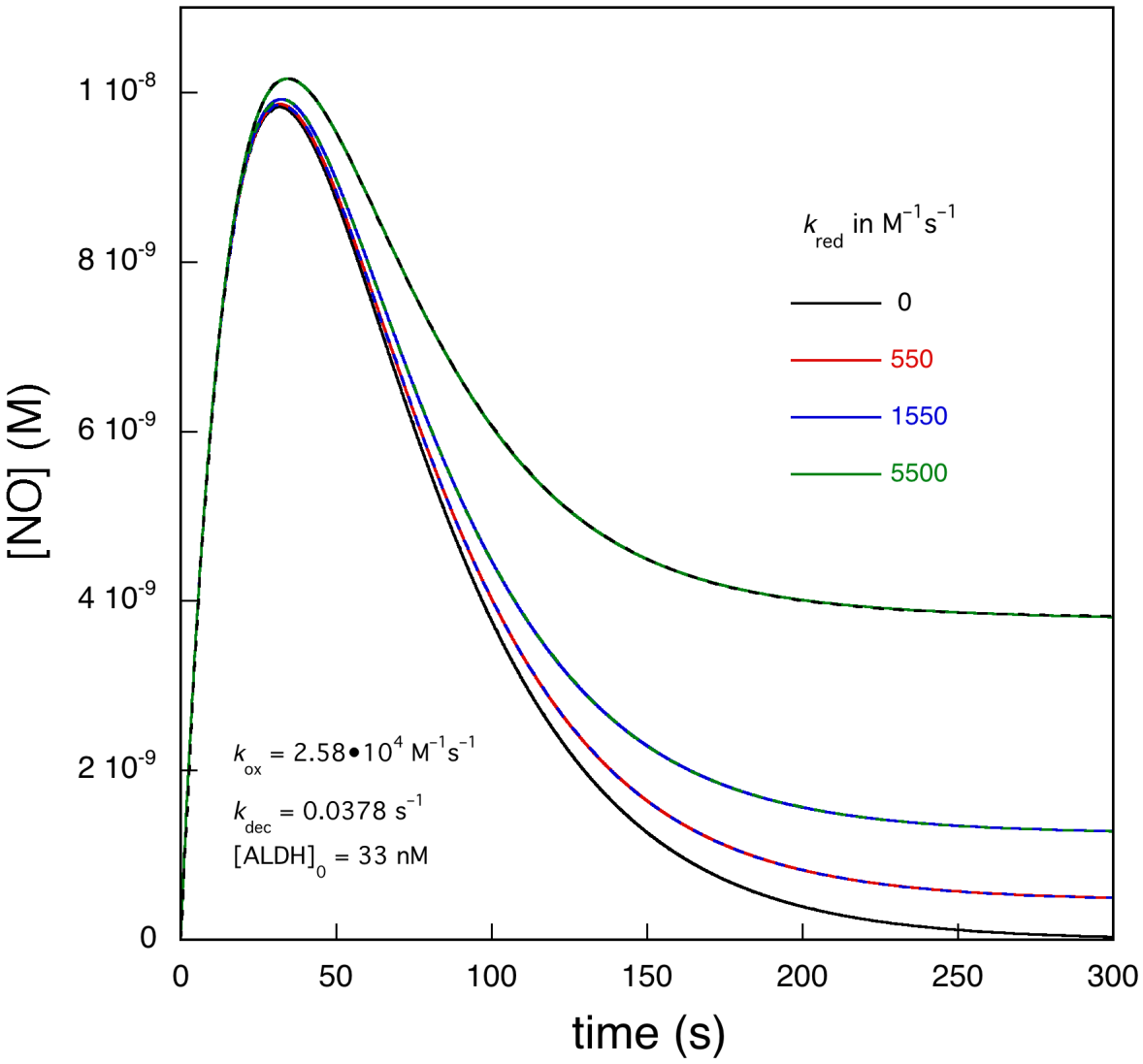
1 10-8
8 10-9
6 10-9
4 10-9
2 10-9
0
[NO] (M)
0
50
100
150
200
250
300
time (s)
kred in M-1s-1
0
550
1550
5500
kox = 2.58•10^4 M-1s-1
kdec = 0.0378 s-1
[ALDH]0 = 33 nM

Table S1 Comparison between simulation and fitting parameters from Fig. S1[a]

Simulation/Fit				
$k_{ox}(s^{-1})$	k_{dec} (s^{-1})	[ALDH] (nM)	v_{cat}[b](nM/s)	R
0.1/0.100	0.02/0.0200	10/9.987	0/0.000	1
0.1/0.103	0.02/0.0199	10/9.620	0.0200/0.0195	1
0.1/0.119	0.02/0.0196	10/8.327	0.0990/0.0884	1.0000
0.1/0.126	0.02/0.0071	10/7.836	0.106/0.0587	0.9998
0.1/n.d.[c]	0.02/0.0209	10/ n.d.[c]	0.990/1.0122	1.0000

[a] Very similar fitted and simulated parameters (less than 10 % difference) are shown in blue. Very different parameters (more than 25 % difference) are shown in red.

[b] The simulated value of v_{cat} was calculated as $v_{cat} = k_{ox} \bullet k_{red} \bullet [ALDH]/(k_{ox}+k_{red})$.

[c] n.d.: not defined. This fit yielded parameters for k_{ox} and [ALDH] with extremely large errors.

Table S2 Comparison between simulation and fitting parameters from Fig. S2[a]

Simulation/Fit				
$k_{ox}(s^{-1})$	k_{dec} (s^{-1})	[ALDH] (nM)	v_{cat}[b](nM/s)	R
0.0258/0.0245	0.0378/0.0396	33/34.6	0/0.000	1
0.0258/0.0249	0.0378/0.0402	33/34.1	0.0178/0.0186	1
0.0258/0.0253	0.0378/0.0415	33/33.5	0.0483/0.0521	1
0.0258/0.0256	0.0378/0.0482	33/32.9	0.1496/0.1833	1

[a] Very similar fitted and simulated parameters (less than 10 % difference) are shown in blue. All differences were smaller than 25 %.

[b] The simulated value of v_{cat} was calculated as $v_{cat} = k_{ox} \bullet k_{red} \bullet [ALDH]/(k_{ox}+k_{red})$.

Figure S3. Comparison of the simulated time courses for NO generation and ALDH oxidation by GTN.

The figure shows the same and a couple of additional simulations as in Fig. S1 with direct comparison of the time courses of NO generation and $ALDH_{red}$. It illustrates that equilibration between the two redox states of ALDH, i.e. the realization of a steady-state is much faster ($k_{obs} \sim k_{ox} \bullet k_{red}/(k_{ox}+k_{red})$ than the rate with which the NO concentration approaches a constant value ($k_{obs} \sim k_{dec}$). Simulations were carried out for a range of values for k_{red} and fixed values of all other parameters: $[GTN]_0$: 10^{-5} M; $[R_{red}]_0$: 10^{-5} M; $[ALDH2_{red}]_0$: 10^{-8} M; k_{ox}: 10^4 $M^{-1}s^{-1}$; k_{dec}: 0.02 s^{-1}; k_{red}: as indicated in the figure panels. Concentrations of GTN were increased 10-fold above 1 mM to prevent depletion within 300 s; to keep the product of $[GTN]_0$ and k_{ox} (i.e. the rate of Rxn 1) constant, k_{ox} was lowered 10-fold concomitantly.

Figure S3

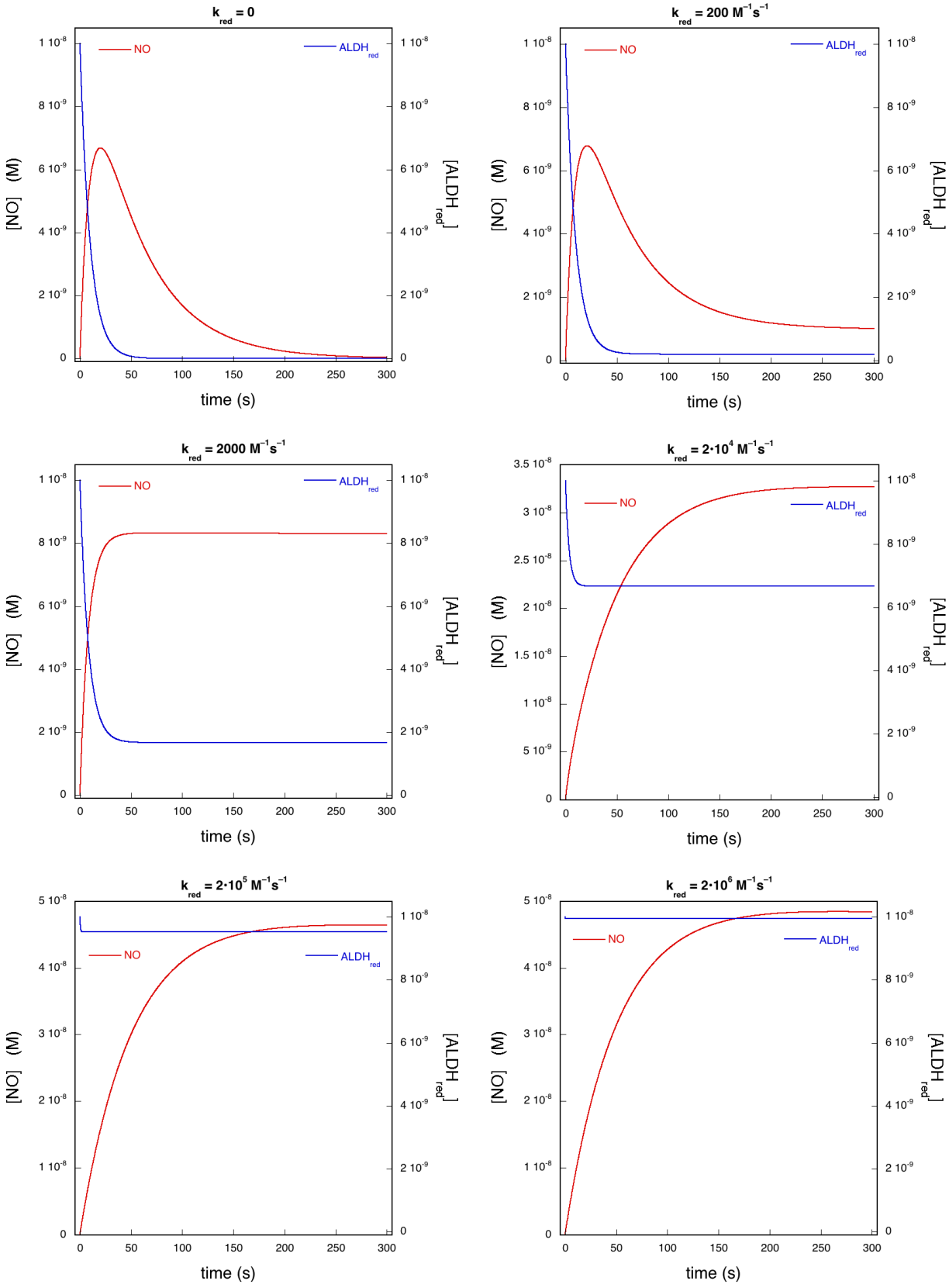
k red = 0
k red = 200 M−1s−1
k red = 2000 M−1s−1
k red = 2·10^4 M−1s−1
k red = 2·10^5 M−1s−1
k red = 2·10^6 M−1s−1
NO
ALDH red
[NO] (M)
[ALDH red] (M)
time (s)

Detailed kinetic analysis: Fitting parameters of average curves vs. average parameters of fits to single curves

To check if the model described by Rxns 1-3 can explain the observed time traces and to obtain estimates for the parameters involved, we took two different approaches. In one approach we averaged all traces (28 for the time courses in the absence of DTT, 13 in its presence) and fitted the average traces to the indicated equations. Alternatively, we fitted all single curves separately and averaged the obtained fitting parameters.

The first method is certainly preferable for presentation purposes. However, a major disadvantage of this method is that the dispersion of the average curve is not translated into the standard deviation/error of the fitting parameters. The latter merely indicates the variation of the fitting parameters that results in acceptable fits to the average curve. For the second method, in contrast, the dispersion parameters (standard deviations/errors) do represent the observed variability of the fitting parameters. However, by this method many time traces did not yield well-defined fitting parameters, even though the fits were excellent. This occurss when the fitting parameter of NO decay (k_{dec}) approaches (or surpasses) the parameter of NO formation (k_{ox}). Since such fits will not contribute to the calculated averages, the fitting parameters obtained by this method may be skewed towards curves with $k_{ox}>>k_{dec}$. This important drawback does not apply to the first method, which truly fits the average of all single traces.

An additional problem is that the fitting parameters are interdependent, in that changes in one parameters away from the best-fit values can be compensated for over a wide range by changes in the other parameters. Therefore, we created tolerance plots for each of the four fitting parameters (see below).

Fitting of the average curves

Eq. 4 yielded excellent fits to the averaged time courses in the absence and presence of DTT (black lines in Fig. S4). The decay of the NO signal in the presence of DTT upon termination of perfusion could be fit to a single exponential (Eq. 3). As mentioned above, the parameters derived from fits to Eq. 4 do not represent unique solutions, since quite substantial variations in any of the four parameters can be compensated for by changes in the other three.

By contrast, this is not the case for the rate constant derived with Eq. 3 for the decay of the NO signal in the presence of DTT upon termination of perfusion (the green time course in Fig. S4). Therefore, assuming that the NO decay rates after termination of perfusion and during perfusion are similar (see below), we refitted the time courses in the presence and absence of DTT with k_{dec} fixed at 2.27 min^{-1}. This yielded an almost identical fit to the time course in the absence of DTT (red line in Fig. S4). A good fit to the time course in the presence of DTT was obtained as well (dark blue line in Fig. S4), but inspection of the fitting parameters showed that the burst phase (k_{ox}•$[ALDH_{red}]_0$, 19 nM/min) was slower than the steady-state phase (v_{cat}, 64 nM/min) and the value of $[ALDH_{red}]_0$ was unreasonably high. This indicates that the burst phase of NO formation disappeared from the fit in the presence of DTT, suggesting that re-reduction of the oxidized enzyme by DTT is faster than oxidation by GTN. Therefore, we fitted the time course for NO formation in the presence of DTT to Eq. 2, which is simpler and in this case more appropriate. This yielded a good fit as well, but with a value for k_2 well below the expected lower limit of 2.27 min^{-1} (orange line in Fig. S4). Refitting the data to Eq. 2 with k_{dec} fixed at 2.27 min^{-1} yielded a rather poor fit (violet line in Fig. S4). Specifically, the slow constant rise in [NO] after the first 2 min was not fitted well under those conditions. A better fit was obtained with a semi-empirical equation consisting of Eq. 2 with an extra linear component (Eq. 2'):

$$[\mathrm{NO}]_t = \frac{v_{cat}}{k_{dec}} \bullet (1 - e^{-k_{dec} \bullet t}) + v \bullet t \qquad \text{(Eq. 2')}$$

The fitting results are summarized in Table S4.

To determine the range of fitting parameters yielding acceptable results we fitted the average time course in the absence of DTT for each of the 4 parameters with a range of fixed values. By visual inspection of the observed fits we estimate that fits become inadequate at values of the correlation coefficient R lower than 0.99 (see Fig. S5). This yielded parameter ranges of 0.6 $min^{-1} < k_{ox} < 5.0\ min^{-1}$, 0.6 $min^{-1} < k_{dec} < 5.0\ min^{-1}$, 14 nM < $[ALDH_{red}]_0$ < 100 nM, and v_{cat} < 4 nM/min. Fixing k_{dec} to 2.27 min^{-1} narrowed the range of the other parameters to 1.1 $min^{-1} < k_{ox} < 2.1\ min^{-1}$, 27 nM < $[ALDH_{red}]_0$ < 41 nM, and v_{cat} < 3.1 nM/min.

Figure S4. Analysis of the average kinetics of formation and decay of NO.

Kinetic analysis was carried out with data from Fig. 4, main text. The red curve shows the average trace for the first perfusion with GTN in the absence of DTT. The blue curve shows the average trace for the first perfusion with GTN in the presence of DTT. The green curve shows the average trace for the decay of signal after cessation of the first perfusion with GTN in the presence of DTT. To account for small variations in the starting/cessation times of perfusion, starting times (t = 0) of individual curves were adapted based on visual inspection before averaging. To account for small variations in initial fluorescence levels the first ~20 data points of individual curves before start of perfusion were averaged and taken as ΔI_{fluor} = [NO] = 0 (blue and red traces only). The green line through the green data points was fit to Eq. 3. Black lines through the red and blue data points were fit to Eq. 4 (the black line through the data in the absence of DTT is almost completely obscured by the red line). The red and blue lines are best fits to Eq. 4 with k_{dec} fixed at 2.27 min^{-1} (the blue line is almost completely obscured by the light blue line). The orange line was fit to Eq. 2. The violet line was fit to Eq. 2 with k_{dec} fixed at 2.27 min^{-1}. The light blue line was fit to Eq. 2 with an extra linear component and k_{dec} fixed at 2.27 min^{-1}. Fitting parameters are presented in Table S3.

Fig. S4

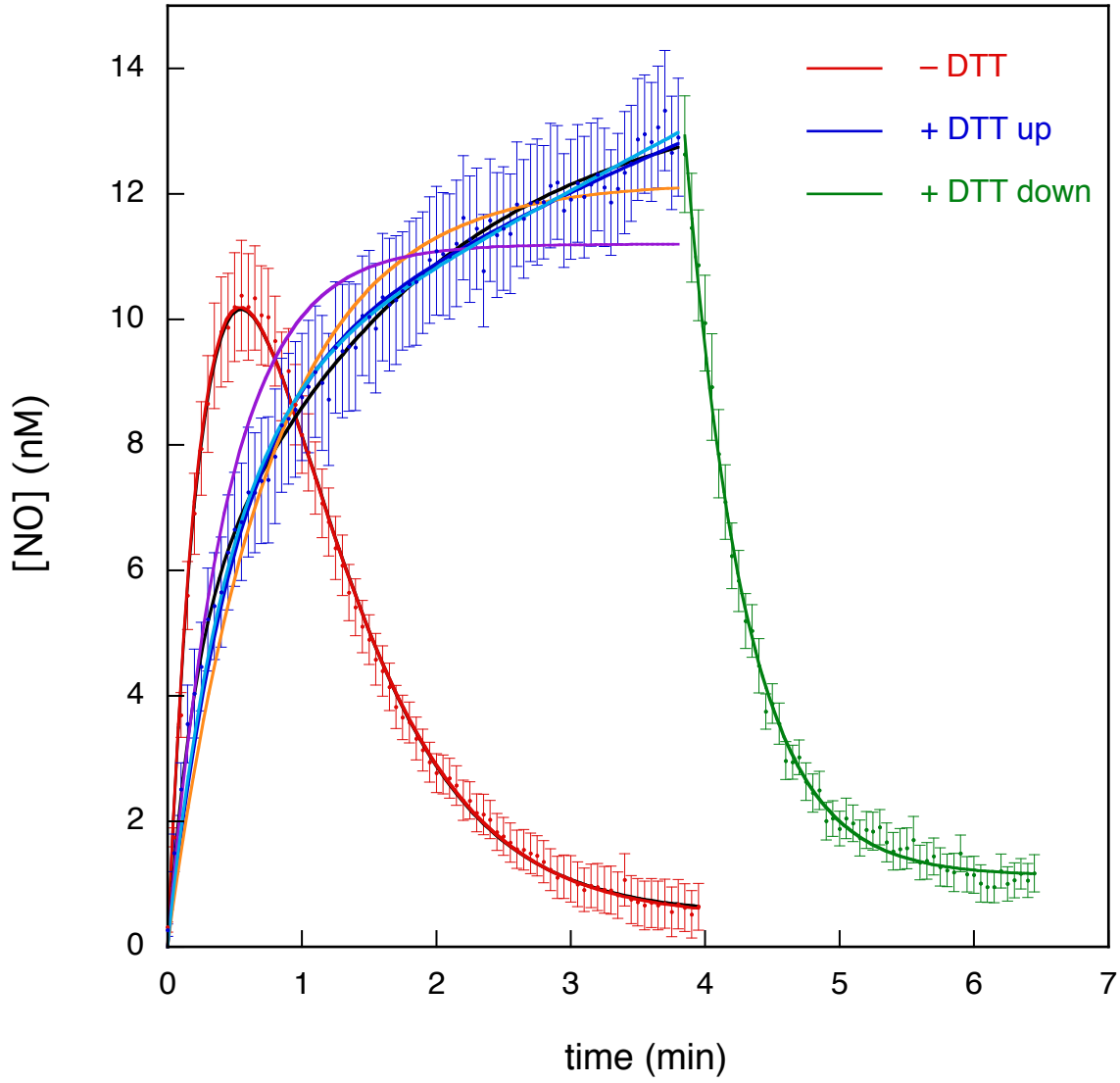

Table S3. Fitting parameters derived from Fig. S4

time course	equation	k_{ox}	k_{dec}	$[ALDH_{red}]_0$[a]	v_{cat}	R
		min^{-1}	min^{-1}	nM	nM/min	
– DTT	4	1.9±2.0[d]	1.8±2.0[d]	27±28[d]	1.0±1.1[d]	0.999
"	4	1.55±0.02	≡ 2.27	33.3±0.3	1.07±0.10	0.999
+ DTT up	4	7.0±0.8	0.59±0.05	4.1±0.3	8.1±0.6	0.997
"	4	0.06±0.05[e]	≡ 2.27	318±285[e]	64±35[e]	0.994
"	2	-	1.31±0.05[f]	-	16.0±0.5	0.98
"	2	-	≡ 2.27	-	25.4±0.3	0.94
"	2'[b]	-	≡ 2.27	-	19.6±0.2	0.995
+ DTT down	3[c]	-	2.27±0.04	-	-	0.998

[a] $[ALDH_{red}]_0$ is the maximal amplitude of the NO signal that would be attained in the absence of decay. According to the proposed model it corresponds to the concentration of available $ALDH2_{red}$.

[b] Eq. 2' yields an additional (empirical) parameter (v = 1.15±0.04 nM/min).

[c] Eq. 3 yields two additional fitting parameters: ΔA = 11.80±0.11 nM and A_∞ = 1.14±0.04 nM, which are the change in amplitude and the final amplitude of the NO signal upon termination of perfusion, respectively.

[d] For this fit no well-defined parameters were obtained.

[e] For this fit the product of k_{ox} and $[ALDH_{red}]_0$, representing the burst phase, was smaller than or equal to the steady-state rate v_{cat}; also, the value of $[ALDH_{red}]_0$ was unreasonably high and ill-defined.

[f] For this fit the value of k_{dec} was smaller than the expected lower limit, 2.27 min^{-1}.

Figure S5 Tolerance plots for the fitting parameters of the average time course in the absence of DTT to Eq. 4.

The central panels show from top to bottom the dependence of the correlation coefficient R for variations in k_{ox}, $[ALDDH_{red}]_0$, and v_{cat} with k_{dec} free (red curves) and fixed to 2.27 min^{-1} (blue curves). The left and right panels show the corresponding fits to lower and higher fitting parameters with R = 0.990 (with k_{dec} fixed). The tolerance plot for k_{dec} (not shown) was identical to that of k_{ox} with k_{dec} free.

Figure S5

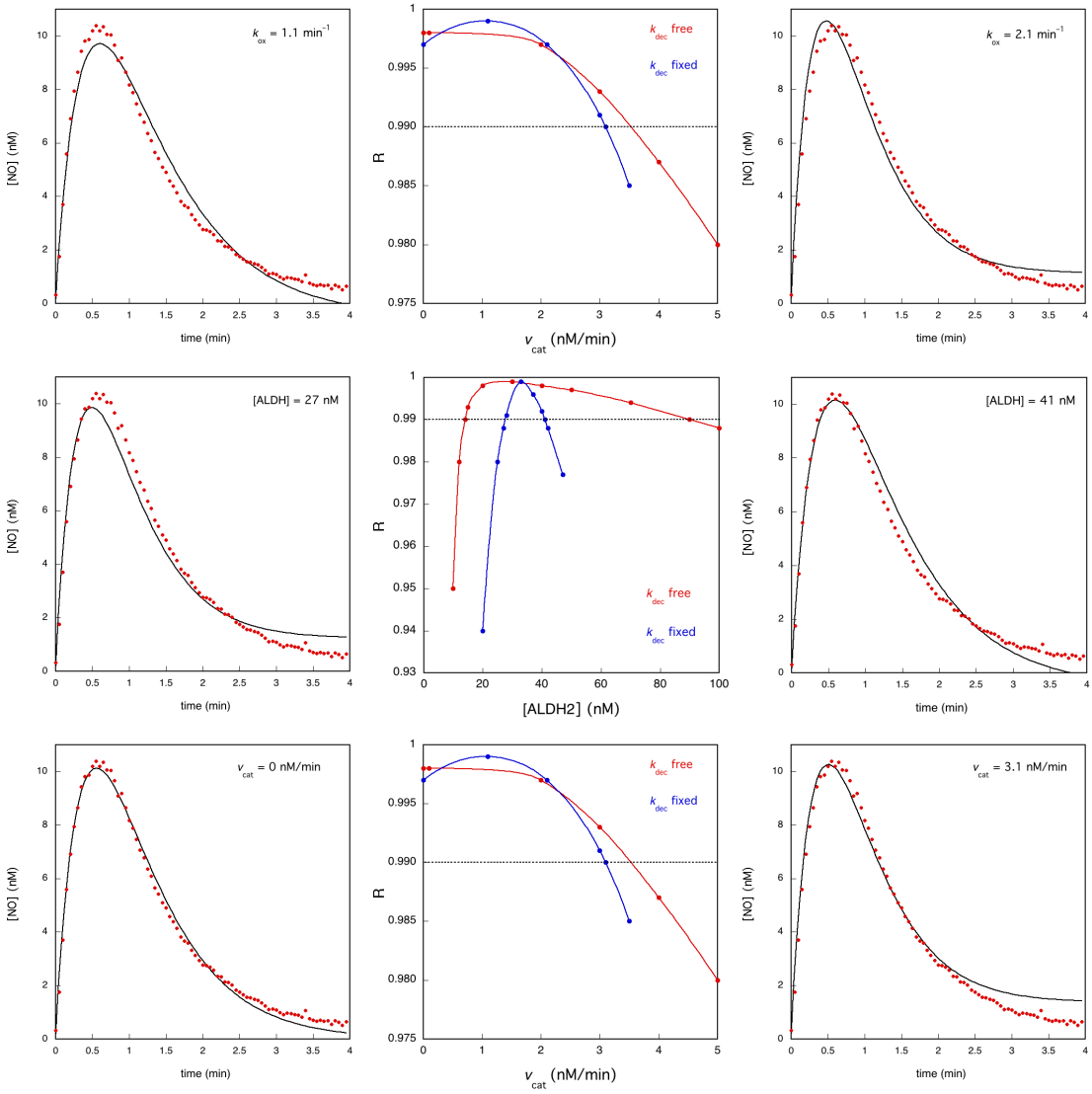
k_{ox} = 1.1 min^{-1}
[NO] (nM)
time (min)
k_{dec} free
k_{dec} fixed
R
v_{cat} (nM/min)
k_{ox} = 2.1 min^{-1}
[ALDH] = 27 nM
[ALDH2] (nM)
[ALDH] = 41 nM
v_{cat} = 0 nM/min
v_{cat} = 3.1 nM/min

Averaging the fitting parameters of separate curves

Although all 28 time courses in the absence of DTT could be fitted to Eq. 4 ($R \geq 0.93$), 11 fits did not yield well-defined values for the four parameters. The distribution of the parameters for the remaining fits is shown in Fig. S6A. We obtained the following average parameters (± SEM): k_{ox} = 5.1±0.5 min^{-1}, k_{dec} = 1.07±0.12 min^{-1}, [ALDH$_{red}$]$_0$ = 8.3±1.0 nM, and v_{act} = 0.9±0.3 nM/min. Notably, a Mann-Whitney test of v_{act} vs. 0 yielded p = 0.011, suggesting a non-zero steady-state activity for ALDH-catalyzed NO generation from GTN. Fitting the NO decay after cessation of perfusion in the presence of DTT to Eq. 3 yielded a value for k_{dec} of 1.98±0.12 min^{-1}. Since this value is little affected by the other parameters of Eq. 3, unlike the strongly interdependent parameters of Eq. 4, and since k_{dec} during perfusion is expected to be equal to or greater than the value after perfusion (see discussion below), we refitted all curves with k_{dec} fixed at 1.98 min^{-1}. With this restriction all curves yielded estimates for the fitting parameters, with values k_{ox} = 2.5±0.2 min^{-1}, [ALDH$_{red}$]$_0$ = 17±3 nM, and v_{act} = 1.1±0.6 nM/min. As can been seen from Fig. S6A, the main effect of fixing k_{dec} is a decrease of k_{ox} and an increase of [ALDH$_{red}$]$_0$. Additionally, the variability of the parameters increased, which can be ascribed to the contribution of the 11 additional time traces. A Mann-Whitney test of v_{act} vs. 0 yielded p = 0.018, again suggesting a non-zero steady-state activity.

Fitting the traces observed in the presence of DTT to Eq. 4 yielded the parameters shown in Fig. S6B, which exhibit unacceptably low values for k_{dec} and [ALDH$_{red}$]$_0$: k_{ox} = 6.4±0.7 min^{-1}, k_{dec} = 0.60±0.18 min^{-1}, [ALDH$_{red}$]$_0$ = 2.0±0.8 nM, and v_{act} = 3.5±1.4 nM/min. Particularly, the low value for [ALDH$_{red}$]$_0$ suggests that a clear burst can no longer be discerned. Fixing k_{dec} at 1.98 min^{-1} resulted in less adequate fits, with R falling below 0.90 in 6 cases, a pronounced increase of v_{cat}. Additionally, it further lowered [ALDH$_{red}$]$_0$ and increased the variability of k_{ox}, indicative of the disappearance of the burst phase (k_{ox} = 9.7±1.2 min^{-1}, [ALDH$_{red}$]$_0$ = 0.9±0.4 nM, and v_{act} = 9.9±0.9 nM/min). Consequently, we fitted the data to Eq. 2, which lacks the burst phase, instead (Fig. S6C). This resulted in reasonable fits but quite a large spread in fitting parameters (k_{dec} = 2.1±0.5 min^{-1} and v_{act} = 12±3 nM/min). Fixing k_{dec} at 1.98 min^{-1} yielded rather poor fits with 6 R values below 0.90 and a more compact series of values for the steady-state activity (v_{act} = 10.4±1.0 min^{-1}).

Figure S6 Distribution of fitting parameters for single NO time courses

The left hand side of Panel A show the distribution of the parameters for fits of the time courses in the absence of DTT to Eq. 4. Only those 17 time traces that yielded well-defined fitting parameters were utilized. The right hand side shows the fitting parameters for all 28 time traces obtained with k_{dec} fixed at 1.98 min^{-1}, which is the mean value obtained for the decay of the NO signal after perfusion in the presence of DTT. Two values for $[ALDH]_0$' (73±17 and 51±5 nM) were outside of the range shown. The left hand side of Panel B show the distribution of the parameters for fits of the 13 time courses in the presence of DTT to Eq. 4. The right hand side shows the corresponding parameters with k_{dec} fixed at 1.98 min^{-1}. The left hand side of Panel C shows the distribution of the parameters for fits of the 13 time courses in the presence of DTT to Eq. 2. The right hand side shows the corresponding parameters with k_{dec} fixed at 1.98 min^{-1}. The estimated decay rate constants for NO observed after cessation of perfusion in the presence of DTT are shown in all three panels as shown as '+ DTT down'.

Figure S6

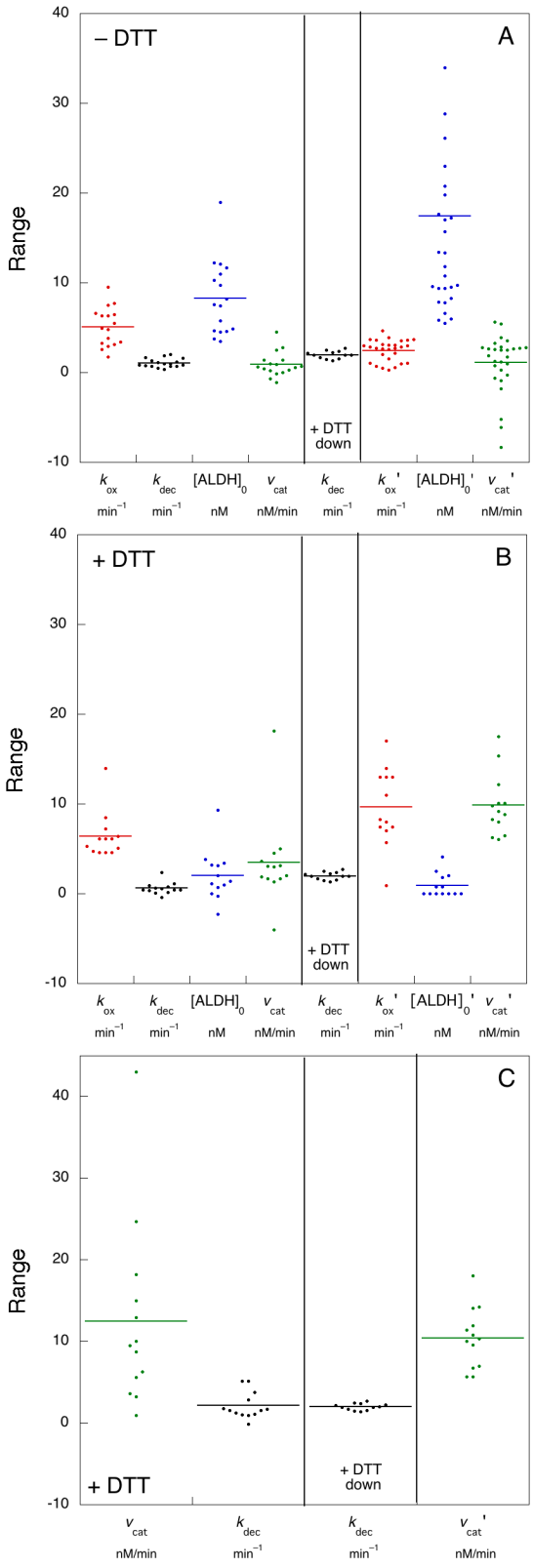
– DTT
A
+ DTT
B
+ DTT
C
Range
40
30
20
10
0
-10
+ DTT down
k_{ox} min^{-1}
k_{dec} min^{-1}
$[ALDH]_0$ nM
v_{cat} nM/min
k_{dec} min^{-1}
k_{ox}' min^{-1}
$[ALDH]_0'$ nM
v_{cat}' nM/min

Identification of the relevant reaction steps

Taken together, the fitting results suggest a burst phase of 1.5-2.5 min^{-1} in the absence of DTT. This rate corresponds to the reaction between $ALDH2_{red}$ and GTN and, since the GTN concentration of 1 µM is much lower than the reported K_m (Chen et al., 2002; Beretta et al., 2008a; Beretta et al., 2010), it constitutes a pseudo-first-order rate constant from which a second-order rate constant of ~$3•10^4$ $M^{-1}•s^{-1}$ can be calculated. The estimated amplitude of the burst phase corresponds to the concentration of $ALDH2_{red}$ and suggests a concentration of 2-4•10^{-8} M C301S/C303S-ALDH2 in the VSMCs. The value of v_{cat} (~1.1 nM/min) represents the slow endogenous regeneration of $ALDH2_{red}$ and corresponds to a turnover number of 0.03-0.06 min^{-1} or 0.5-1.0•10^{-3} s^{-1} (calculated as $v_{cat}/[ALDH_{red}]_0$).

For the reaction in the presence of DTT we estimate a value for v_{cat} of 10-20 nM/min, which is 10-to-20x higher than in the absence of DTT. Because of the consumption of NO by DTT (Fig. 2, main text), this may still be an underestimation by ~43 %, suggesting that DTT increases the turnover number ~15-to-25-fold. The value of the turnover number with GTN and DTT that can be estimated amounts to 0.5-0.7 min^{-1}, which agrees reasonably well with values reported with the purified enzyme of 0.45 min^{-1} (Beretta et al. 2008b).

As for the rate-limiting reactions, we can rule out diffusion of GTN into the cell as the main contributing factor for the rise of the NO signal. Although diffusion is a first-order process, NO formation would be limited by the availability of $ALDH2_{red}$, and since the GTN concentration is much higher than the ALDH2 concentration, rate-limiting GTN diffusion would result in a linear increase of [NO] that ends abruptly when all ALDH2 is oxidized. Combined with the subsequent decay the resulting time course would be clearly different from the observed ones. Moreover, it would require that the rate constant for diffusion of GTN into the cell be at least two orders of magnitude slower than the rate constant for diffusion out of the cell, which seems unreasonable.

For the decay of the NO signal after termination of perfusion we obtained a $t_{1/2}$ of approx. 20 s. To identify the step(s) responsible for this reaction we make two assumptions: (i) the rates of diffusion of GTN in and out of the cell are similar and (ii) the rate of diffusion of NO out of the cell is at least as fast as that of GTN. In that case, after termination of perfusion, synthesis of NO will stop because of diffusion of GTN out of the system. Decay of the NO signal cannot be faster than the latter process. Consequently, assuming that the

diffusion rates of GTN and NO are similar, the observed decay can be equated to the rate of NO diffusion out of the system. Decay during perfusion (k_{dec} in the fits) will be due to the same process, possibly in combination with consumption of NO by cellular components. NO autoxidation can be ruled out to make a significant contribution, since, at the observed NO concentrations of 15 nM or less, NO autoxidation at 37 °C will result in a half-life of > 7 hrs (estimated with $k = 1.36 \cdot 10^7$ $M^{-2}s^{-1}$ and $[O_2]$ = 185 µM; Ford et al., 1993; Schmidt et al., 1997). Depending on the contribution of NO consumption, decay during perfusion will thus be equally fast as or faster than decay after termination of perfusion, and the rate constant of 2.27(1.98) min^{-1} for NO decay observed after termination of perfusion can be considered to be a lower limit for NO decay during perfusion (k_{dec}). To get an estimate for the contribution of other reactions to NO decay during diffusion, we fitted the observed time course (in the absence of DTT) with increasing values of k_{dec} and found that fits became inacceptable for values above approx. 3.5 min^{-1} (results not shown). Consequently, we conclude that NO consumption contributes 1/3 or less to the overall NO decay rate during perfusion (k_{dec}). As loss of NO due to perfusion does not occur in the relaxation studies, we estimate that the steady-state concentration of NO in those experiments was at least 3x higher.

Fitting the decay after termination of perfusion required a non-zero final level of NO (A_∞). Although we cannot rule out that this is due to baseline drift, it is conceivable that it is caused by slow NO release by nitrosothiols formed by intermediacy of DTT during perfusion with GTN (see above). Such DTT-related side reactions may also be to blame for the rather unsatisfactory fit (R=0.94) we obtained in the presence of DTT after fixing k_{dec} to 2.27 min^{-1}, and thus cause the apparent linear increase in [NO] at times above 2 min.

Figure S7 Individual traces that were averaged in Fig. 1A

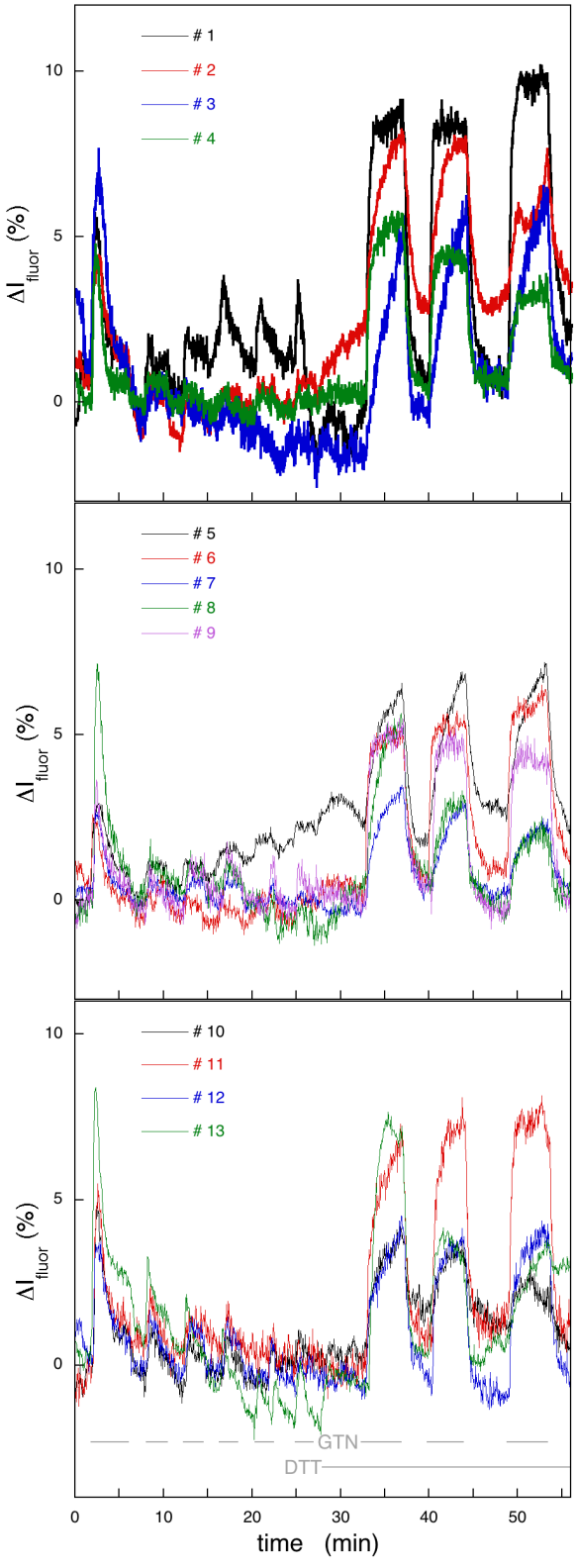

Figure S8 Individual traces that were averaged in Fig. 6A

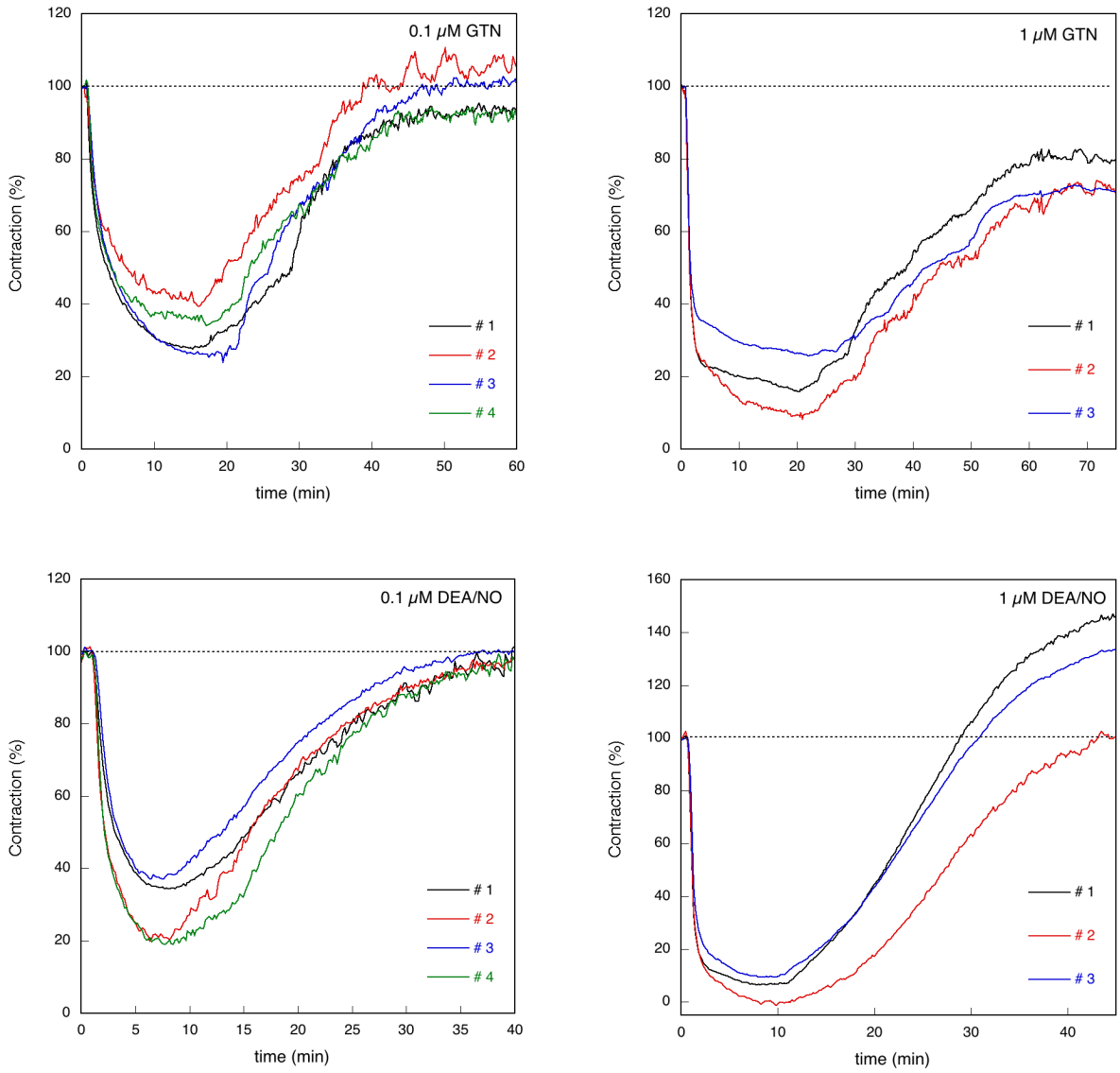

Statistical tests *(for easier orientation p values have been marked with different colours: red: $p \leq 0.05$; blue: $0.05 < p \leq 0.10$; black: $p > 0.10$)*

Fig. 1A: The changes in NO concentrations occurring upon cessation or initiation of perfusion were tested with a paired *t*-test. To this end the NO levels before and after the events were each averaged over a period of 30 s. Then the pre- and post-event average values obtained in this way were compared for all single curves ($n = 13$). The resulting *p*-values were:

1st perfusion	cessation	$p < 0.0001$
2nd perfusion	initiation	$p < 0.0001$
2nd perfusion	cessation	$p = 0.00017$
3rd perfusion	initiation	$p < 0.0001$
3rd perfusion	cessation	$p < 0.0001$
4th perfusion	initiation	$p < 0.0001$
4th perfusion	cessation	$p < 0.0001$
5th perfusion	initiation	$p = 0.040$
5th perfusion	cessation	$p < 0.0001$
6th perfusion	initiation	$p = 0.00014$

Fig. 3A: The amplitudes of the average curves of the experiments ($n = 3$) were tested by ANOVA followed by Dunnett's post-hoc test against the initial amplitude as control.

ANOVA: $p < 0.0001$

Dunnett:

2nd vs. 1st:	$p = 0.864$
3rd vs. 1st:	$p = 0.164$
4th vs. 1st:	$p = 0.009$
5th vs. 1st:	$p = 0.003$
6th vs. 1st:	$p < 0.0001$

Figure S9 Decrease of the NO signal in the presence of DTT upon repeated perfusion (data from Fig. 3A)

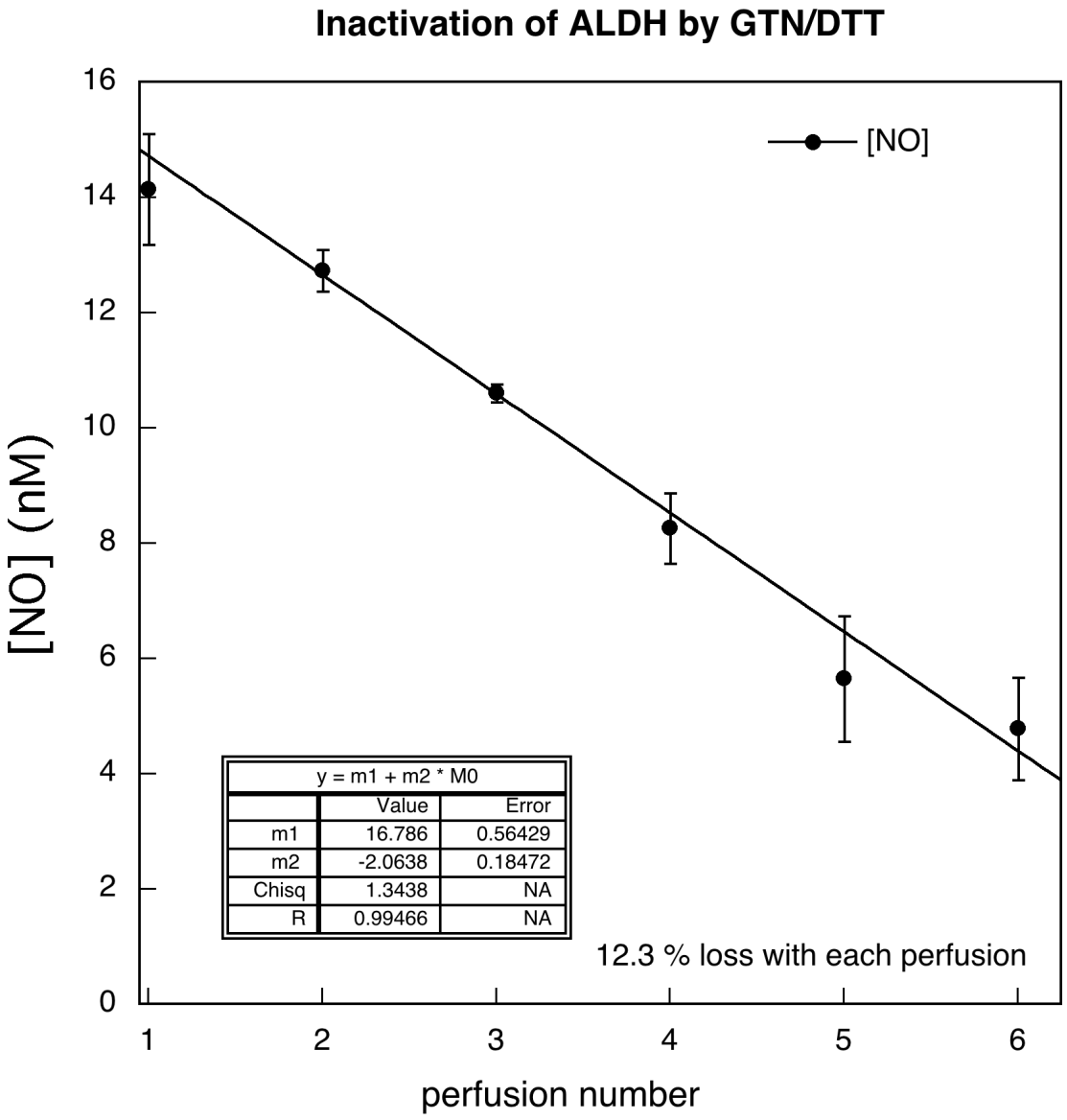

Fig. 4: The fitting parameter v_{cat} was fitted against 0 with the Mann-Whitney test.

with k_{dec} free: $p = 0.011$; with k_{dec} fixed: $p = 0.018$ (see above, p. S19).

Fig. 5: The NO peak heights and ALDH2 expression levels were tested by ANOVA followed by Dunnett's post-hoc test against the initial value as control.

Fig. 5A:	ANOVA:	$p = 0.0095$	Dunnett:	1hr vs. ctrl.: $p = 0.014$
				3hr vs. ctrl.: $p = 0.324$
				6hr vs. ctrl.: $p = 0.856$
Fig. 5B:	ANOVA:	$p = 0.024$	Dunnett:	1hr vs. ctrl.: $p = 0.024$
				3hr vs. ctrl.: $p = 0.889$
				6hr vs. ctrl.: $p = 0.999$
Fig. 5C:	– cycloheximide:	ANOVA:	$p = 0.58$	
	+ cycloheximide:	ANOVA:	$p = 0.75$	
Fig. 5D:	ANOVA:	$p = 0.060$	Dunnett:	1hr vs. ctrl.: $p = 0.058$
				3hr vs. ctrl.: $p = 0.049$
				6hr vs. ctrl.: $p = 0.093$

idem + cycloheximide (Fig. S11)

Fig. S11:	ANOVA:	$p = 0.023$	Dunnett:	1hr vs. ctrl.: $p = 0.028$
				3hr vs. ctrl.: $p = 0.029$
				6hr vs. ctrl.: $p = 0.020$

Figure S10. Effect of perfusion with chloralhydrate on the generation of NO from GTN. C301S/C303S-ALDH2 overexpressing VSMC were perfused with 1 µM GTN or 10 µM DEA/NO as indicated in the absence (black) and presence (red) of 1 mM chloral hydrate and the NO concentration was monitored by fluorescence microscopy (n = 4, with 16 and 18 traces in the absence and presence of chloral hydrate, respectively). See Materials & Methods for further details. In the presence of chloral hydrate NO was observed during perfusion with DEA/NO but not with GTN.

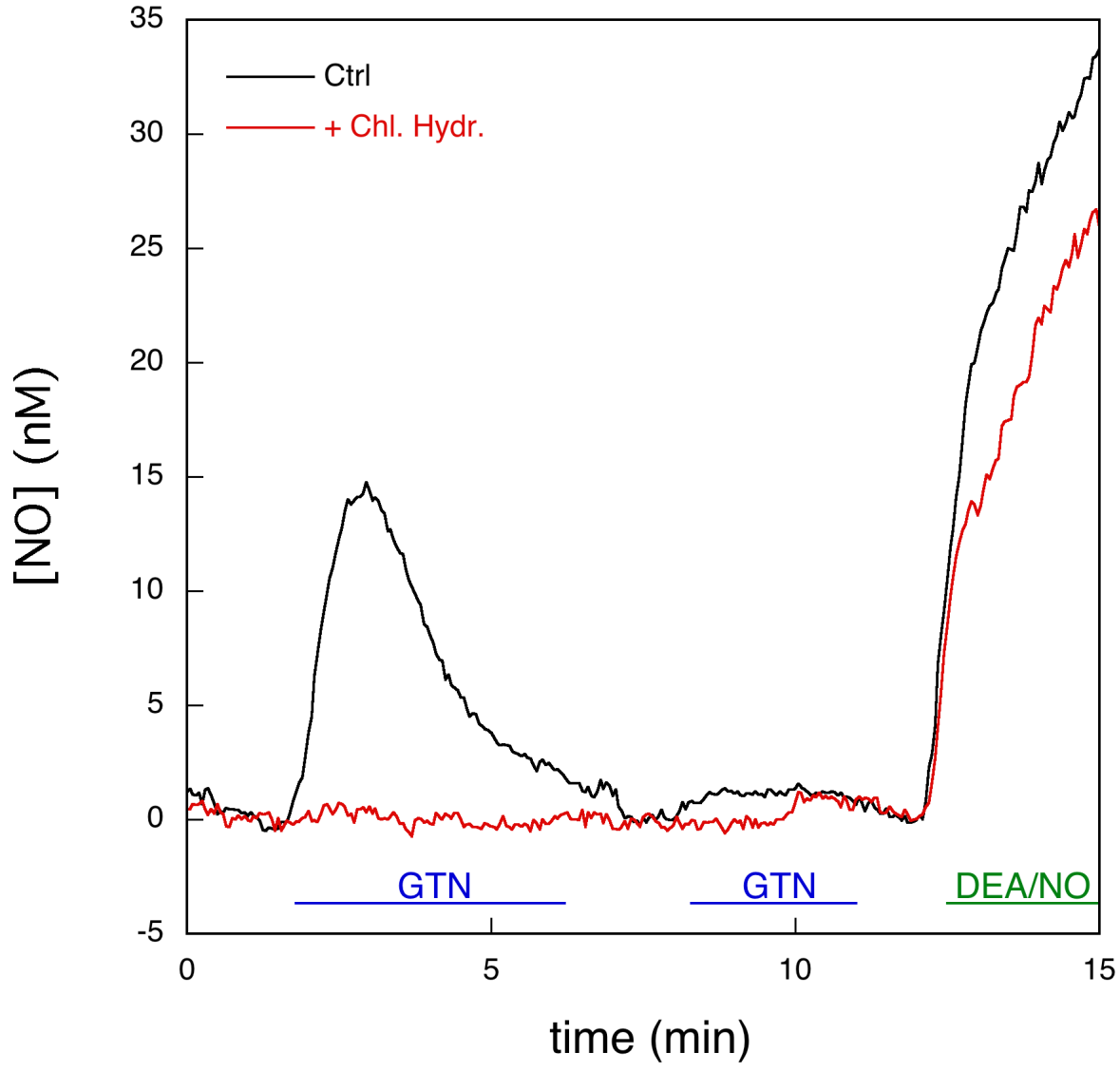

Figure S11. The irreversibility of loss of NO generation upon perfusion with GTN and DTT is not affected by cycloheximide.

Experimental conditions as for Fig. 5D of the main text, except for the presence of 10 μg/mL cycloheximide (n = 3).

Figure S11

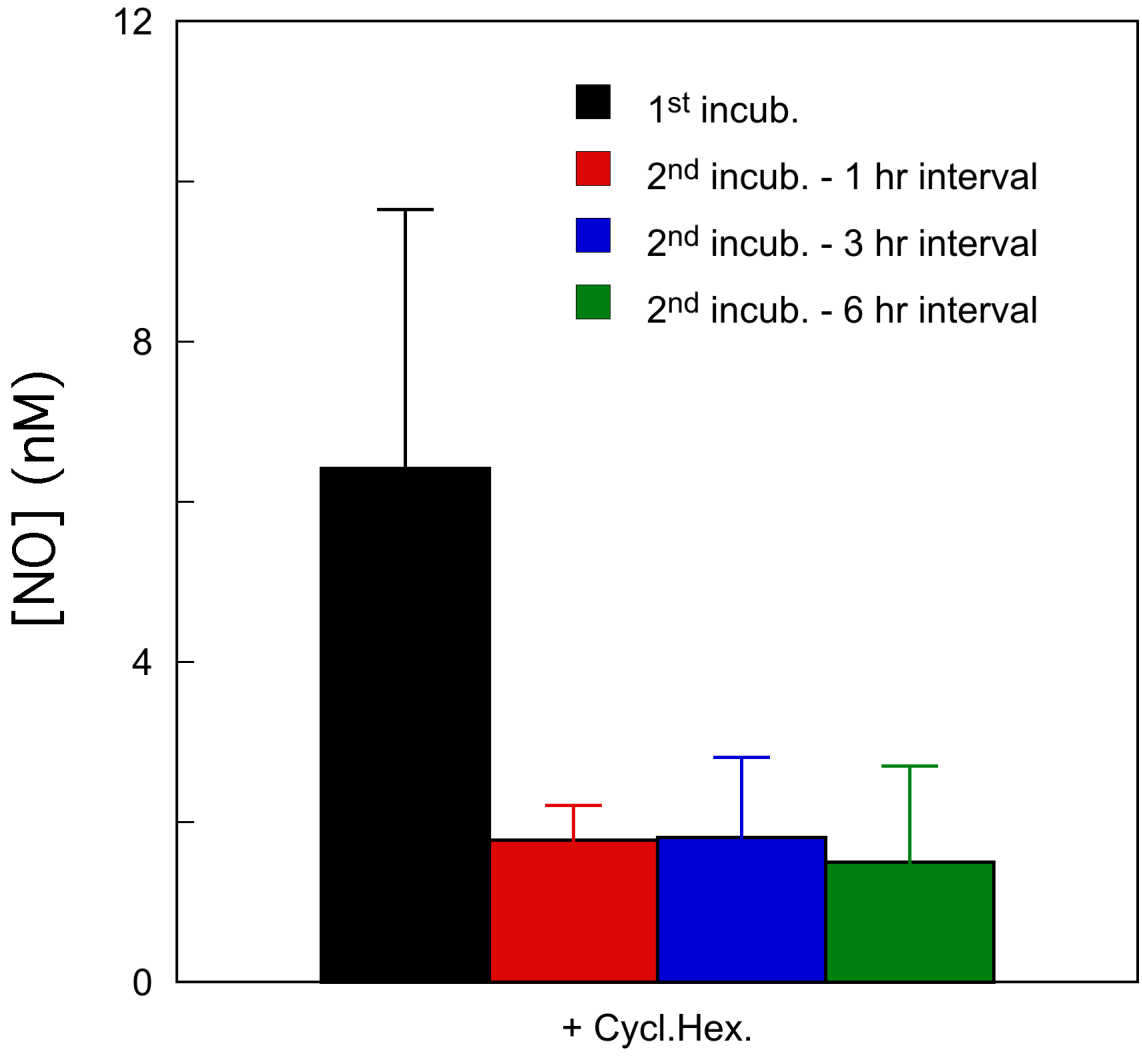

Figure S12. Effect of PX-12 on NO generation from GTN. C301S/C303S-ALDH2 overexpressing VSMC were perfused with 1 μM GTN or 10 μM DEA/NO as indicated after preincubation for 24 hrs in the absence (black) or presence (red) of the irreversible inhibitor of thioredoxin PX-12 (10 μM) and the NO concentration was monitored by fluorescence microscopy (n = 7, with 32 and 31 traces in the absence and presence of PX-12, respectively). See Materials & Methods for further details. PX-12 did not affect NO generation.

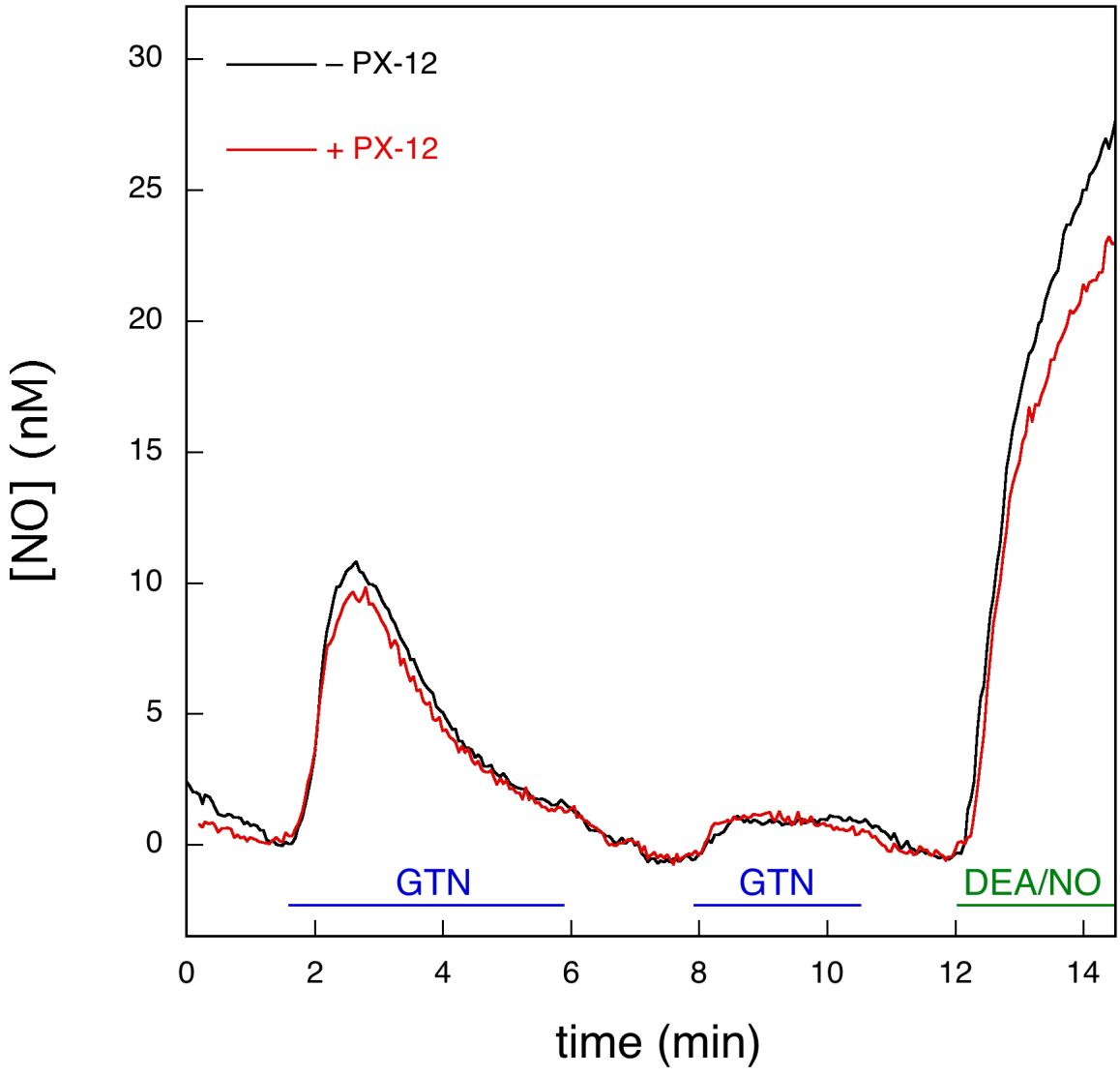

References

Beretta, M, Gruber, K, Kollau, A, Russwurm, M, Koesling, D, Goessler, W, Keung, WM, Schmidt, K, and Mayer, B (2008a) Bioactivation of nitroglycerin by purified mitochondrial and cytosolic aldehyde dehydrogenases. *J Biol Chem* **283:** 17873-17880.

Beretta, M, Sottler, A, Schmidt, K, Mayer, B, and Gorren, ACF (2008b) Partially irreversible inactivation of mitochondrial aldehyde dehydrogenase by nitroglycerin. *J Biol Chem* **283:** 30735-30744.

Beretta, M, Gorren, ACF, Wenzl, MV, Weis, R, Russwurm, M, Koesling, D, Schmidt, K, and Mayer, B (2010) Characterization of the East Asian variant of aldehyde dehydrogenase-2. Bioactivation of nitroglycerin and effects of Alda-1. *J Biol Chem* **285:** 943-952.

Chen, Z, Zhang, J, and Stamler, JS (2002) Identification of the enzymatic mechanism of nitroglycerin bioactivation. *Proc Natl Acad Sci USA* **99:** 8306-8311.

Ford, PC, Wink, DA, and Stanbury, DM (1993) Autoxidation kinetics of aqueous nitric oxide. *FEBS Lett* **326:** 1-3.

Opelt, M, Eroglu, E, Waldeck-Weiermair, M, Russwurm, M, Koesling, D, Malli, R, Graier, WF, Fassett, JT, Schrammel, A, and Mayer, B (2016) Formation of nitric oxide by aldehyde dehydrogenase-2 is necessary and sufficient for vascular bioactivation of nitroglycerin. *J Biol Chem* **291:** 24076-24084.

Schmidt, K, Desch, W, Klatt, P, Kukovetz, WR, and Mayer, B (1997) Release of nitric oxide from donors with known half-life: A mathematical model for calculating nitric oxide concentrations in aerobic solutions. *Naunyn Schmiedebergs Arch Pharmacol* **355:** 457-462.